

# Geochemistry, Geophysics, Geosystems®



## RESEARCH ARTICLE

10.1029/2023GC011222

## Preliminary Characterization of Submarine Basalt Magnetic Mineralogy Using Amplitude-Dependence of Magnetic Susceptibility

### Key Points:

- Paleomagnetic studies utilize either alternating field or thermal demagnetization, but it is difficult to choose the best protocol a priori
- Amplitude-dependence of magnetic susceptibility measurements permits preliminary magnetic mineralogy characterization in submarine basalts
- Rapid amplitude-dependence measurements may aid in deciding upon the best demagnetization protocol for submarine basalt samples

### Correspondence to:

H. Yang,  
[hyang777@stanford.edu](mailto:hyang777@stanford.edu)

### Citation:

Yang, H., Tikoo, S. M., Carvalho, C., Bilardello, D., Solheid, P., Gaastra, K. M., et al. (2024). Preliminary characterization of submarine basalt magnetic mineralogy using amplitude-dependence of magnetic susceptibility. *Geochemistry, Geophysics, Geosystems*, 25, e2023GC011222. <https://doi.org/10.1029/2023GC011222>

Received 8 SEP 2023  
Accepted 1 JAN 2024  
Corrected 15 FEB 2024
















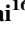





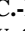






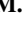




This article was corrected on 15 FEB 2024.  
See the end of the full text for details.

### Author Contributions:

**Conceptualization:** H. Yang, S. M. Tikoo  
**Data curation:** H. Yang, C. Carvalho, D. Bilardello, P. Solheid, K. M. Gaastra, S. Thoram, K. Hoernle, T. W. Höfig, A. Avery, A. V. Del Gaudio, Y. Huang, R. Bhutani, D. M. Buchs, C. Class, Y. Dai, G. Dalla Valle, S. Fielding, S. Han, D. E. Heaton, S. Homrighausen, Y. Kubota, C.-F. Li, W. R. Nelson, E. Petrou, K. E. Potter, S. Pujatti, J. Scholpp, J. W. Shervais, M. Tshiningayamwe, X. J. Wang, M. Widdowson

© 2024 The Authors. *Geochemistry, Geophysics, Geosystems* published by Wiley Periodicals LLC on behalf of American Geophysical Union.

This is an open access article under the terms of the [Creative Commons Attribution-NonCommercial License](https://creativecommons.org/licenses/by/4.0/), which permits use, distribution and reproduction in any medium, provided the original work is properly cited and is not used for commercial purposes.

H. Yang<sup>1,2</sup> , S. M. Tikoo<sup>1,2</sup> , C. Carvalho<sup>3</sup> , D. Bilardello<sup>4</sup> , P. Solheid<sup>4</sup> , K. M. Gaastra<sup>5,6</sup> , W. W. Sager<sup>5</sup> , S. Thoram<sup>5</sup> , K. Hoernle<sup>7</sup> , T. W. Höfig<sup>8,9</sup> , A. Avery<sup>10</sup> , A. V. Del Gaudio<sup>11</sup> , Y. Huang<sup>12</sup> , R. Bhutani<sup>13</sup> , D. M. Buchs<sup>14</sup> , C. Class<sup>15</sup> , Y. Dai<sup>16</sup> , G. Dalla Valle<sup>17</sup> , S. Fielding<sup>18</sup> , S. Han<sup>19</sup> , D. E. Heaton<sup>20</sup> , S. Homrighausen<sup>7</sup> , Y. Kubota<sup>21</sup> , C.-F. Li<sup>22</sup> , W. R. Nelson<sup>23</sup> , E. Petrou<sup>24</sup> , K. E. Potter<sup>25</sup> , S. Pujatti<sup>26</sup> , J. Scholpp<sup>27</sup> , J. W. Shervais<sup>25</sup> , M. Tshiningayamwe<sup>28</sup> , X. J. Wang<sup>29</sup> , and M. Widdowson<sup>30</sup> 

<sup>1</sup>Department of Geophysics, Stanford University, Stanford, CA, USA, <sup>2</sup>Department of Earth and Planetary Sciences, Stanford University, Stanford, CA, USA, <sup>3</sup>UMR 7590, Institut de Minéralogie, de Physique des Matériaux et de Cosmochimie, Sorbonne Université, Paris, France, <sup>4</sup>Institute for Rock Magnetism, University of Minnesota, Minneapolis, MN, USA, <sup>5</sup>Department of Earth and Atmospheric Sciences, University of Houston, Houston, TX, USA, <sup>6</sup>NASA Jet Propulsion Laboratory, California Institute of Technology, Pasadena, CA, USA, <sup>7</sup>GEMAR Helmholtz Centre for Ocean Research Kiel, Kiel, Germany, <sup>8</sup>International Ocean Discovery Program, Texas A&M University, College Station, TX, USA, <sup>9</sup>Project Management Jülich, Jülich Research Centre GmbH (FZJ), Rostock, Germany, <sup>10</sup>School of Geosciences, University of South Florida, Tampa, FL, USA, <sup>11</sup>Department of Earth Sciences (Geology and Paleontology), University of Graz, NAWI Graz Geocenter, Graz, Austria, <sup>12</sup>Key Laboratory of Exploration Technologies for Oil and Gas Resources (Yangtze University), Ministry of Education, Wuhan, China, <sup>13</sup>Department of Earth Sciences, Pondicherry University, Puducherry, India, <sup>14</sup>School of Earth and Environmental Sciences, Cardiff University, Cardiff, UK, <sup>15</sup>Lamont-Doherty Earth Observatory, Columbia University, Palisades, NY, USA, <sup>16</sup>Department of Geology, Lund University, Lund, Sweden, <sup>17</sup>Institute for Marine Sciences, National Research Council, Bologna, Italy, <sup>18</sup>Geology Department, University of Namibia, Windhoek, Namibia, <sup>19</sup>School of Environmental Science and Technology, Gwangju Institute of Science and Technology, Gwangju, South Korea, <sup>20</sup>CEOAS, Oregon State University, Corvallis, OR, USA, <sup>21</sup>Department of Geosciences, Penn State University, State College, PA, USA, <sup>22</sup>Ocean College, Zhejiang University, Zhoushan, China, <sup>23</sup>Department of Physics, Astronomy & Geosciences, Towson University, Towson, MD, USA, <sup>24</sup>Department of Earth Sciences, University of Oxford, Oxford, UK, <sup>25</sup>Department of Geosciences, Utah State University, Logan, UT, USA, <sup>26</sup>Department of Geoscience, University of Calgary, Calgary, AB, Canada, <sup>27</sup>Department of Earth and Planetary Sciences, University of Tennessee, Knoxville, TN, USA, <sup>28</sup>Geology Department, University of Namibia, Keetmanshoop, Namibia, <sup>29</sup>Department of Geology, Northwest University, Xi'an, China, <sup>30</sup>School of Environmental Sciences, University of Hull, Hull, UK

**Abstract** The past ~200 million years of Earth's geomagnetic field behavior have been recorded within oceanic basalts, many of which are only accessible via scientific ocean drilling. Obtaining the best possible paleomagnetic measurements from such valuable samples requires an a priori understanding of their magnetic mineralogies when choosing the most appropriate protocol for stepwise demagnetization experiments (either alternating field or thermal). Here, we present a quick, and non-destructive method that utilizes the amplitude-dependence of magnetic susceptibility to screen submarine basalts prior to choosing a demagnetization protocol, whenever conducting a pilot study or other detailed rock-magnetic characterization is not possible. We demonstrate this method using samples acquired during International Ocean Discovery Program Expedition 391. Our approach is rooted in the observation that amplitude-dependent magnetic susceptibility is observed in basalt samples whose dominant magnetic carrier is multidomain titanomagnetite (~TM<sub>60-65</sub>, (Ti<sub>0.60-0.65</sub>Fe<sub>0.35-0.40</sub>)Fe<sub>2</sub>O<sub>4</sub>). Samples with low Ti contents within titanomagnetite or samples that have experienced a high degree of oxidative weathering do not display appreciable amplitude dependence. Due to their low Curie temperatures, basalts that possess amplitude-dependence should ideally be demagnetized either using alternating fields or via finely-spaced thermal demagnetization heating steps below 300°C. Our screening method can enhance the success rate of paleomagnetic studies of oceanic basalt samples.

**Plain Language Summary** Oceanic basalts are ideal recorders of the Earth's magnetic field. To decipher magnetic histories recorded in rocks, paleomagnetists need to isolate the magnetization directions and intensities within rocks by one of two possible methods. One method typically involves progressively heating the samples to high temperatures. The other method involves exposing samples to alternating magnetic fields with increasing peak field intensities. Both of these methods are ultimately destructive to the original

**Formal analysis:** H. Yang, C. Carvallo

**Funding acquisition:** S. M. Tikoo, D. Bilardello, P. Solheid, K. M. Gaastra, W. W. Sager

**Investigation:** H. Yang, C. Carvallo, D. Bilardello, P. Solheid, K. M. Gaastra, W. W. Sager, S. Thoram, T. W. Höfig

**Methodology:** H. Yang, S. M. Tikoo, C. Carvallo, D. Bilardello, P. Solheid

**Project administration:** H. Yang, S. M. Tikoo

**Resources:** S. M. Tikoo, W. W. Sager

**Supervision:** S. M. Tikoo

**Validation:** H. Yang

**Visualization:** H. Yang

**Writing – original draft:** H. Yang

**Writing – review & editing:** S. M. Tikoo, C. Carvallo, D. Bilardello, P. Solheid, K. M. Gaastra, W. W. Sager, S. Thoram, K. Hoernle, T. W. Höfig, A. Avery, A. V. Del Gaudio, Y. Huang, R. Bhutani, D. M. Buchs, C. Class, Y. Dai, G. Dalla Valle, S. Fielding, S. Han, D. E. Heaton, S. Homrighausen, Y. Kubota, C.-F. Li, W. R. Nelson, S. Petrou, K. E. Potter, S. Pujatti, J. Scholpp, J. W. Shervais, M. Tshiningayamwe, X. J. Wang, M. Widdowson

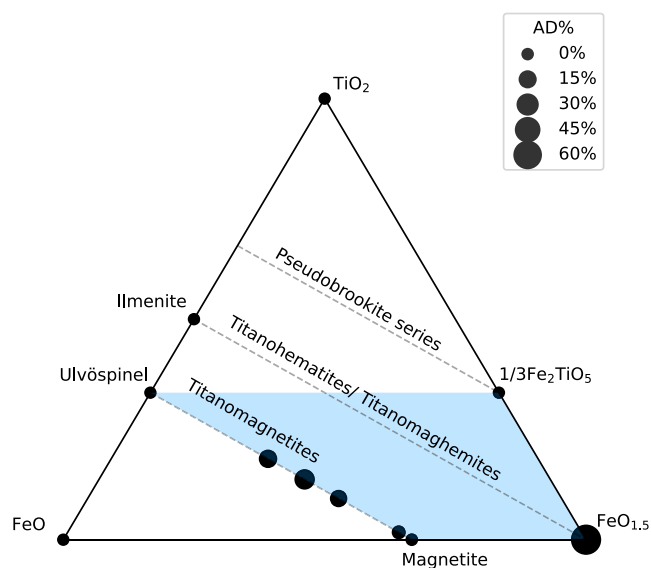
magnetization preserved within rocks. However, without knowledge of a given rock's magnetic mineralogy, randomly choosing thermal or alternating field demagnetization methods may result in high failure rates. We developed a pre-screening method to help decide which cleaning method will likely be more successful for a given sample based on low-field magnetic susceptibility measurements. These measurements do not affect the original magnetic information recorded in a rock, thereby permitting subsequent paleomagnetic studies on the same sample. Our technique can be performed as rapidly as 2 min per sample, is non-destructive, and does not require complicated sample preparation.

## 1. Introduction

Oceanic basalts are a database of Earth's magnetic field records, preserving information about the intensity and geometry of the geodynamo field over time. Observations of magnetic stripes within the ocean floor have provided key insights into the processes of geomagnetic reversals, seafloor spreading, and plate tectonics (e.g., Gee & Kent, 2007; Vine & Matthews, 1963). Oceanic basalt ages obtained using geochronology and magnetostratigraphy may be used to constrain the speed of subduction as well as the deformation in the Earth's oceanic crust (e.g., Kreemer & Gordon, 2014). Meanwhile, the paleolatitudes of ancient islands and seamounts have been reconstructed to constrain the motion of hotspots, which is driven by flows in the Earth's mantle (Bono, Tarduno, & Bunge, 2019; Tarduno et al., 2003) or alternatively, the extent of true polar wander (e.g., Sager, 2007; Sager & Koppers, 2000). Paleomagnetic studies aimed at understanding the nature and timing of geomagnetic reversals, paleointensity variations, and secular variation serve to produce the primary data sets required to test theories of Earth's core composition, thermal and mechanical evolution, and dynamo behavior (Bono, Tarduno, Nimmo, & Cottrell, 2019; Tauxe, 2006).

To conduct paleomagnetic studies on oceanic basalts, scientific ocean drilling expeditions are often necessary to obtain samples. With newly acquired samples, it is difficult to decide a priori whether alternating field (AF) or thermal demagnetization methods are more suitable due to the complex magnetic mineralogy of submarine basalts (Furuta, 1993; Özdemir, 1987; Zhou et al., 2000). Because AF or thermal treatment demagnetization erases the magnetization, it is desirable to have a fast and non-destructive pre-screening method to determine which demagnetization method is more appropriate. Several factors may limit the possibility of conducting detailed rock magnetic characterization prior to demagnetization experiments. These may include: (a) limited material available from recovered cores, (b) lack of access to requisite instrumentation that would permit investigations into high- and low-temperature magnetic behavior or domain state, and (c) insufficient time to conduct detailed rock magnetic studies. In this study, we explore whether measuring the magnetic field amplitude-dependence of magnetic susceptibility (MS) can be used as a simple and quick way to pre-screen oceanic basalt samples and choose the best demagnetization method and protocols.

For oceanic basalts on Earth, the expected magnetic carriers fall into the compositional space defined by four endmembers: magnetite, ulvöspinel, hematite and pseudobrookite (Figure 1). The magnetite-ulvöspinel solid solution represents fresh submarine basalt, whereas the pseudobrookite-hematite series represents completely oxidized basalt. During basalt crystallization, Ti preferably resides in these Fe-Ti oxide minerals compared to other paramagnetic silicate minerals, and the Ti content in the magnetic minerals depends on the composition of the parental magma. After the formation of basalts, oxidation can occur at low temperatures (below 200°C) (Özdemir, 1987) when seawater transports oxidizing species through cracks within rocks. The oxidation can change the magnetic mineralogy in two ways. First, fresh titanomagnetite would gradually transform into titanomaghemite or titanohematite (Bleil & Petersen, 1983; Zhou et al., 2001). Second, paramagnetic minerals such as olivine and pyroxene can be oxidized to form magnetite or hematite (Gunnlaugsson et al., 2006). Additional complexities may arise due to compositional heterogeneity from exsolution of titanomagnetite (Bowles & Jackson, 2016; Bowles et al., 2019; Xu et al., 1997). All these factors in combination determine the magnetic properties of oceanic basalts, which can make it difficult to pre-select a demagnetization method. Some samples may contain high-coercivity magnetic minerals such as hematite that cannot be easily demagnetized using typical peak AF amplitudes (~20–200 mT) (Bilardello & Roberts, 2020; Roberts et al., 2020). Other samples may be dominated by Ti-rich titanomagnetite with low (<200–300°C) Curie temperatures. In such cases, if the thermal demagnetization steps are too large, there may not be sufficiently high resolution to fit primary magnetization directions using principal component analysis (Kirschvink, 1980), particularly if the magnetization presents overlapping components.



**Figure 1.** FeO-Fe<sub>2</sub>O<sub>3</sub>-TiO<sub>2</sub> ternary diagram. The shaded region shows the possible magnetic mineralogies that can be found in terrestrial submarine basalts. Symbol sizes represent the amplitude-dependence (AD) of magnetic susceptibility (MS) for the different minerals reported in Clark (2016).

Likewise, data resolution may not allow obtaining robust Thellier-Thellier-based paleointensity estimates (Coe, 1967; Tauxe & Staudigel, 2004; Thellier, 1959). Obtaining as much information as possible about the magnetic mineralogy of samples prior to commencing destructive demagnetization experiments is critical to the success of paleomagnetic investigations.

MS is a measure of how easily a material responds to an applied weak magnetic field, which is closely linked to how it acquired a remanent magnetization and how this magnetization behaves when demagnetized in a laboratory. MS may depend on the amplitude of the magnetic field applied and how frequently the field direction changes (Bilardello, 2023; Jackson et al., 1998; Ustra et al., 2018). Alternating current (AC) susceptibility is measured by applying an alternating magnetic field with a specified field intensity (peak value of field amplitude) and frequency. The alignment of the electron spin orientations within a magnetic grain is affected by the properties of the applied field. Since magnetization is a representation of the alignment of electron spins within a sample, the magnetization and its derived MS are time-dependent and this leads to a frequency dependence. This degree of alignment is also related to the domain walls inside a multidomain (MD) grain, which results in an amplitude-dependence. Amplitude-dependence has at times been referred to as field-dependence in the literature (De Wall, 2000; Jackson et al., 1998; Vahle & Kontny, 2005). However, both amplitude and frequency are properties of an AC magnetic field, so that use of the term field-dependence is less specific, and we adopt the terms amplitude-dependence and frequency-dependence throughout this paper.

Jackson et al. (1998) and references therein explained the amplitude-dependence of AC susceptibility for MD titanomagnetite at low fields (i.e., a few hundred A/m). We provide a short summary of these works here for context: Hysteresis of magnetization is commonly observed at strong magnetic fields (~0.5–1 T). Meanwhile, the movement of domain walls within MD grains may produce magnetic hysteresis at low field amplitudes. Domain walls separate different regions with unparallel magnetization within grains. For a MD crystal, the susceptibility value reflects the net sum of the magnetization of all domains divided by applied field amplitude. If the domain walls remain stable for various field amplitudes and all domains respond to externally applied fields equally, the ratio of net magnetization to field amplitude (susceptibility) will remain the same. However, if different domain walls begin to move at different field amplitudes, the net sum of magnetization would be significantly changed. This would result in the measured susceptibility becoming a function of the applied field. Since the application of an external magnetic field would favor the growth of domains with magnetization directions along the direction of the applied field, the amplitude-dependence of susceptibility is typically positive. However, negative amplitude-dependence may also be observed and this behavior is suspected to be due to superparamagnetic magnetite (Hamilton, 2021).

At room temperature, the relationship between amplitude-dependence and composition for titanomagnetites can be explained by the analysis of magnetic energies (Jackson et al., 1998). In a simplified model, three energies are involved in this process: (a) the wall displacement-energy function  $E_w(d)$ , (b) the magnetostatic self-energy  $E_m(d)$ , and (c) the magnetostatic energy associated with the external field  $E_h(d)$ . All these energies are functions of the domain wall displacement ( $d$ ).  $E_w(d)$  is a sinusoidal function that is modulated by defects in the crystal. The local minima of  $E_w(d)$  are the possible positions of domain walls.  $E_w(d)$  appears to be independent of Ti content.  $E_h(d)$  is the driving force of domain wall movement from external fields while  $E_m(d)$  is the resisting force. The gradient of  $E_h(d)$  is proportional to the saturation magnetization ( $M_s$ ), while  $E_m(d)$  is proportional to  $M_s^2 d^2$ . For TM<sub>0</sub> composition, the Ti-free end member of titanomagnetite that has the highest  $M_s$  value in the TM series,  $E_m(d)$  dominates and external fields will not substantially affect domain wall positions. With increasing Ti content,  $M_s$  values gradually decrease, and  $E_m(d)$  decreases much faster than  $E_h(d)$ . When  $E_h(d)$  is comparable to  $E_m(d)$ , domain wall movement can occur and results in an amplitude-dependent susceptibility.

Since low-field amplitude-dependence is associated with the domain wall motion, single-domain grains of all magnetic minerals are supposed to be amplitude independent. In this case, we need to consider the upper critical

single-domain size-limit of each mineral. For fresh titanomagnetite ( $TM_{55-60}$ ), the critical SD grain size is  $0.4 \pm 0.2 \mu\text{m}$ , while for partially oxidized titanomagnetite, this threshold rises to  $1.55 \pm 0.8 \mu\text{m}$  (Butler & Banerjee, 1975; Dunlop & Özdemir, 1997; Moskowitz, 1980). Therefore, fresh titanomagnetite has a wider grain size range to become MD and therefore amplitude-dependent. It is worth noting that the formation of maghemite introduces a high density of vacancies in the crystal, which also hinders domain wall motion and causes maghemite-bearing samples to be more amplitude-independent. For comparison, hematite and pyrrhotite have critical SD grain sizes of 15 and 1.6  $\mu\text{m}$ , respectively (Banerjee, 1971; Dunlop & Özdemir, 1997; Soffel, 1977). Both of these minerals have been reported as amplitude-dependent in prior studies (Clark, 2016; Worm et al., 1993). Magnetite has a critical SD size of 0.05–0.084  $\mu\text{m}$  (Dunlop, 1973; Dunlop & Özdemir, 1997), but its large magnetostatic energy (associated with  $M_s$ ) would prevent the domain wall motion during MS measurements, even when in a multi-domain state. The amplitude-dependence of MD minerals in the Ti-Fe-O compositional range from previous studies is summarized in Figure 1.

Though the magnetic mineralogy of terrestrial submarine basalts and the amplitude-dependence of individual minerals have been extensively investigated, few studies have focused on applying this method to natural rocks to infer the magnetic mineralogy. In this study, we focus on the amplitude-dependence of MS of submarine basalt samples. We test this method on a suite of samples collected from a recent scientific ocean drilling expedition and explore whether it may be used as a non-destructive pre-screening method to decide the most appropriate demagnetization method for individual oceanic basalt samples in situations where more detailed preliminary rock magnetic characterization and/or pilot studies cannot be performed.

## 2. Materials and Methods

### 2.1. Sample Descriptions

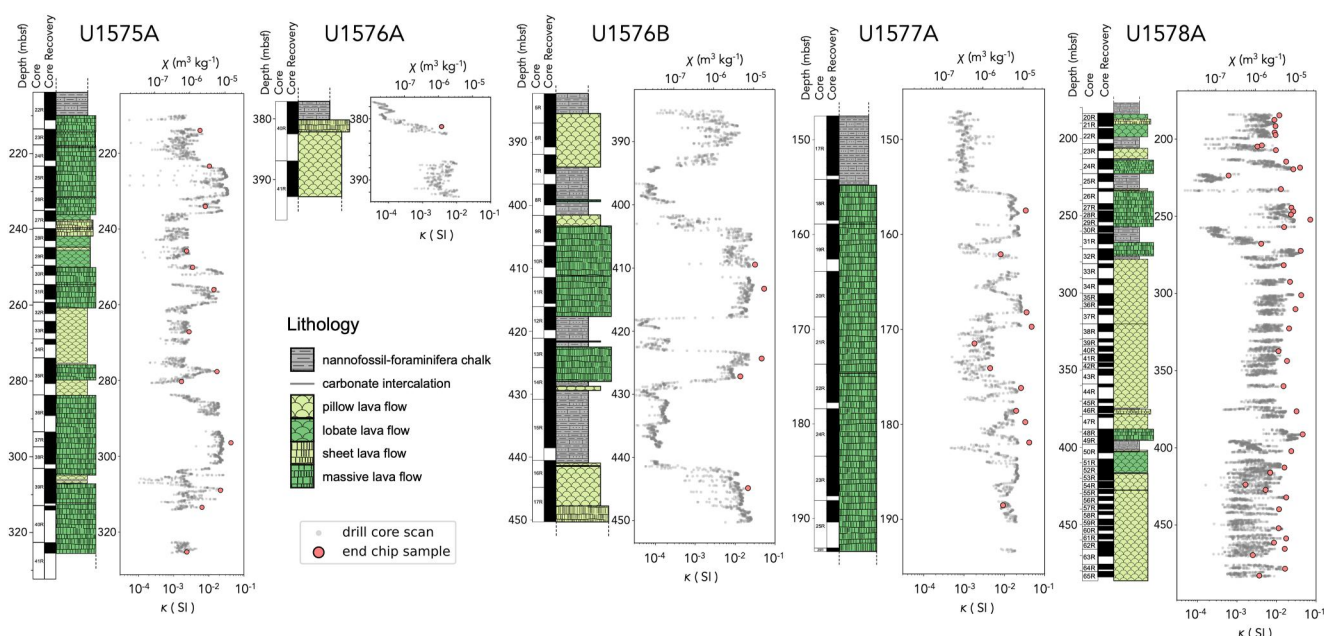
Samples used in this study are submarine basalts collected from the Walvis Ridge (Tristan-Gough) hotspot track in the southern Atlantic Ocean during International Ocean Discovery Program (IODP) Expedition 391 (Sager et al., 2022, 2023). These basalts were obtained from five holes (U1575A, U1576A, U1576B, U1577A, and U1578A) with approximate ages spanning 100–63 Ma (Figure 2). Two types of samples were used in this study: oriented rock cubes with a volume of 8  $\text{cm}^3$  for paleomagnetic investigation, and their adjacent end chips (same depth unoriented saw cutting residues) with variable masses/volumes for rock magnetic measurements.

Submarine basalts can be classified into pillow lavas, which are small cooling units that are often fractured, and massive or sheet flows, which are thicker and usually contain fewer fractures. The classification was documented by petrologists on board during IODP Expedition 391 (Sager et al., 2022, 2023). Examination of hand samples reveals that weathering is common in our samples, as evidenced by the presence of olivine grains transformed into iddingsite through seawater penetration and low-temperature fluid-rock interactions (Sager et al., 2022, 2023). However, fresh and relatively unweathered samples can be found within massive and sheet flows, likely because of their dense and homogeneous nature. Similarly, if pillow lava grow rapidly into thick piles of tens of meters, as interpreted for basalts from Hole U1578A (Figure 2), weathering is delayed, preserving some fresh material. For rocks in which olivine alteration can be identified, titanomagnetites have also been affected (e.g., Hole U1575A) (Sager et al., 2022, 2023). At the macroscopic scale, “fresh-looking” hand samples do not guarantee lack of alteration as these samples may contain partially weathered titanomagnetites. The samples used in this study do not contain glassy margins.

### 2.2. Magnetic Characterization

#### 2.2.1. Room Temperature Rock Magnetic Measurements

We performed a series of room-temperature bulk susceptibility measurements on 74 basalt end chips using different amplitudes (30 and 300 A/m) of AC magnetic fields but at a constant frequency (976 Hz). These bulk susceptibility measurements were conducted using an AGICO MFK2-FA Kappabridge magnetic susceptibility meter in the Stanford Paleomagnetism Laboratory. We report mass-normalized susceptibility ( $\chi$ ) throughout the paper except for the continuous core volume susceptibility data in Figure 2. These values were used to derive the amplitude-dependence of each sample. The magnetic susceptibility amplitude-dependence is calculated as  $\chi_{AD} = (\chi_{300 \text{ A/m}} - \chi_{30 \text{ A/m}})/(\chi_{30 \text{ A/m}})$ , following the approach of De Wall (2000) and Clark (2016).



**Figure 2.** Igneous basement section of the five holes drilled during International Ocean Discovery Program Expedition 391, shown with their lithology and magnetic susceptibility. Red dots represent the basalt samples used in this study. We report mass-normalized ( $\chi$ ) susceptibility for discrete samples (red dots) and volume-normalized ( $\kappa$ ) susceptibility for continuous cores (gray dots). Axes were aligned using a mean basalt density of  $2.9 \text{ g cm}^{-3}$ . The MS values of some of the samples are larger than the core values because the whole-round cores include void space that lowers the bulk MS.

We also measured magnetic hysteresis loops and backfield DC demagnetization curves for 38 samples using a Lakeshore 8600 Series vibrating sample magnetometer at the Institute for Rock Magnetism (IRM), University of Minnesota. Additional hysteresis loops and backfield demagnetization data were acquired for 36 basalt samples with a magnetometer ( $\mu$ -VSM) from Princeton Measurements Corporation at the Institut de Physique du Globe (IPGP) - Institut de Minéralogie et de Physique des Milieux Condensés (IMPMP) Mineral Magnetism Analytical Facility. For the hysteresis experiments, we used a peak saturating magnetic field of 1.5 T, a step size of 2 mT and an averaging time of 0.1 s. For the backfield remanence curves, we measured the remanent magnetization from +1.5 T to a field step where the remanent magnetization changes to the opposite direction. From these data, we obtained values for the hysteresis parameters  $M_r$  (remanent magnetization),  $M_s$  (saturation magnetization),  $H_{cr}$  (coercivity of remanence), and  $H_c$  (coercive force).

To further understand the grain sizes and domain states of the magnetic minerals within our samples, we conducted First Order Reversal Curve (FORC) measurements using a Lakeshore 8600 Series vibrating sample magnetometer for a subset ( $n = 19$ ) of basalts. FORCs were measured by first saturating the sample to 0.5 T. The field was then lowered to a reversal field  $H_a$ . Measurements of magnetization, denoted by  $M(H_a, H_b)$ , are taken at various fields  $H_b$  as the applied field increases to positive saturation. These steps are repeated for the next reversal field  $H_a$ , and until  $H_a$  reaches the saturating field. For our FORC measurements, we used an averaging time of 0.1–0.5 s, and a field step size (for  $H_a$  and  $H_b$ ) of 1–1.5 mT. We typically collected and combined 200–450 FORCs for each sample. Differing FORC acquisition protocols were sometimes applied to different samples due to laboratory timing constraints. The FORC function is defined as the mixed second derivative of  $M(H_a, H_b)$ :

$$\rho(H_a, H_b) = -\frac{1}{2} \frac{\partial^2 M(H_a, H_b)}{\partial H_a \partial H_b}$$

The FORC function is plotted in  $H_c - H_i$  coordinates, where  $H_c = (H_b - H_a)/2$ , and  $H_i = (H_a + H_b)/2$ . The distribution along the  $H_c$  axis can be linked to the distribution of micro-coercivities. The physical meaning of  $H_i$  is more complex, but it may represent the degree of interacting fields (in first approximation) for stable SD grains (Roberts et al., 2000, 2014). The FORC data were processed with FORCinel, and a constant smoothing factor of 4 was used for all samples (Harrison & Feinberg, 2008).

### 2.2.2. Low- and High-Temperature Rock Magnetic Measurements

We measured the susceptibility versus temperature ( $\chi$ - $T$ ) curves to determine the thermal stability of the magnetic carriers and derive the Curie temperatures of any thermally stable minerals. The  $\chi$ - $T$  experiments were conducted at the IRM, University of Minnesota and at the Stanford Paleomagnetism Laboratory. Heating curves were measured from room temperature to 650–700°C, followed by the measurement of cooling curves back to 40°C. The  $\chi$ - $T$  curves at Stanford were obtained with a MFK2-FA Kappabridge (with default field amplitude of 200 A/m and frequency of 976 Hz) in an argon atmosphere (ultra-high purity grade). To detect the possible existence of the magnetite Verwey transition or hematite Morin transition, additional low temperature  $\chi$ - $T$  curves were measured from room temperature down to  $-193^{\circ}\text{C}$  before and after the heating treatment using a CS-L low temperature cryostat apparatus. At the University of Minnesota, high-temperature  $\chi$ - $T$  curves were acquired in air using a KLY-2 Kappabridge (with default field amplitude of 300 A/m and frequency of 920 Hz). In total, we collected 35  $\chi$ - $T$  curves in Ar and 30  $\chi$ - $T$  curves in air.

### 2.2.3. Demagnetization Experiments

To examine potential relationships between the amplitude-dependence of MS and the demagnetization behavior of submarine basalts, we performed parallel AF and thermal demagnetization experiments on sister specimens of three of our basalt samples. For the thermal demagnetization experiments on the *JOIDES Resolution*, 8 cm<sup>3</sup> cubic paleomagnetic specimens ( $n = 7$ , see Table 1) were subjected to stepwise heating up to 600°C (at intervals of 50°C from 150 to 250°C and 25°C for higher temperatures). Sample B7151 was treated with stepwise AF demagnetization (peak AF fields at 2, 5, 7, 10, 15, 20, 25, 30, 40, 50, 60, 80 mT). The remanent magnetization remaining after each heating or AF step was then measured using an AGICO JR-6 spinner magnetometer as a part of the routine shipboard measurements aboard the *JOIDES Resolution* drillship during IODP Expedition 391. Our AF demagnetization sister specimens were prepared by collecting unoriented 0.01–0.04 g pieces from the basalt end chips. Note that this end chip sampling was done prior to the rock magnetic thermal experiments, so the AF specimens contain their original NRM. The AF specimens were then glued onto a 2.5 cm diameter nonmagnetic quartz wafer using cyanoacrylate cement. Next, these specimens were subjected to stepwise AF demagnetization using a 2G Enterprises 755 superconducting rock magnetometer in the Stanford Paleomagnetism Laboratory. The magnetometer is located within a Lodestar magnetically shielded room (ambient field  $\sim 200$  nT) and is equipped with automated inline rock magnetic experimental equipment (Kirschvink et al., 2008). Principal component analysis of the obtained stepwise demagnetization was performed to derive the characteristic remanent magnetization (ChRM) (Kirschvink, 1980). A rotation matrix was calculated using the ChRMs of both the oriented cubic sample and the unoriented rock chip sample. All demagnetization steps of the unoriented specimen were rotated by this matrix to better compare with the shipboard measurements on oriented specimens.

## 3. Results

### 3.1. Room Temperature Rock Magnetic Measurements

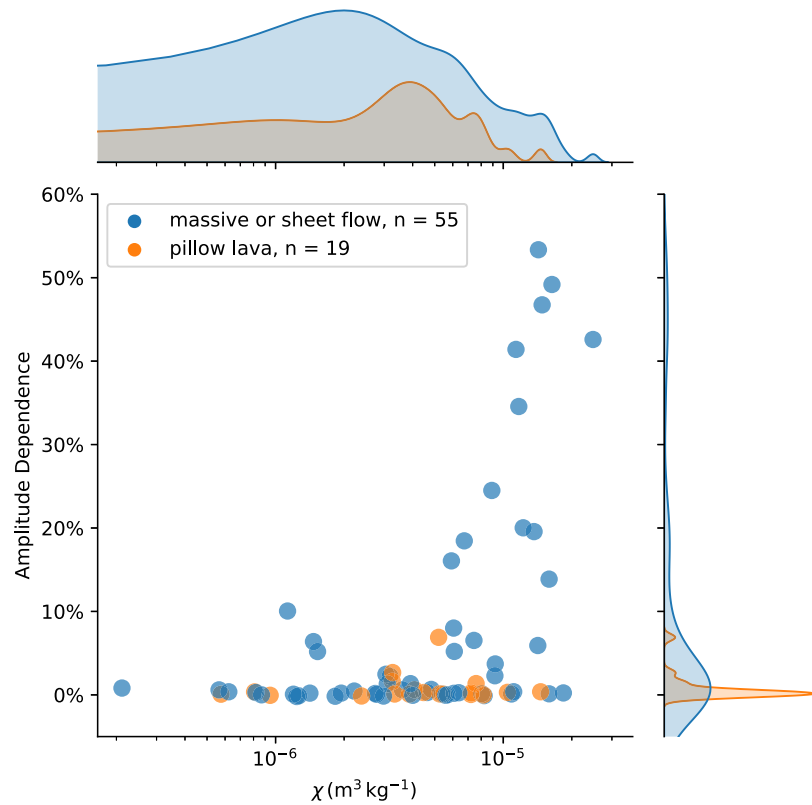
In our collection of submarine basalts, the mass susceptibility ranges from  $2 \times 10^{-7}$  to  $2 \times 10^{-5}$  m<sup>3</sup>/kg. Using a basalt density of  $\sim 2,900$  kg/m<sup>3</sup>, this equals susceptibility in SI of  $6 \times 10^{-4}$  to  $6 \times 10^{-2}$ , consistent with previous reports (e.g., Moskowitz et al., 2015). The amplitude dependence ranges from 0% to 53%. We found that most basalts are amplitude-independent, with all pillow basalts falling into this category. Amplitude-dependence (AD > 10%) is observed only in massive flows. Amplitude-dependent samples also appear to be correlated with high bulk susceptibility ( $> 5 \times 10^{-5}$  m<sup>3</sup> kg<sup>-1</sup>), possibly because the amplitude-dependent samples are dominated by relatively fresh titanomagnetite. In contrast, seawater alteration-induced-maghemitization of titanomagnetite grains will reduce the amplitude-dependence.

In the Day plot (scatter plot of  $M_r/M_s$  against  $H_{cr}/H_c$ ), amplitude-dependent samples (B7151 and B9051, Figures 4h and 4i) are located in the bottom part (Figure 4a) with high  $H_{cr}/H_c$  and low  $M_r/M_s$ . Amplitude-independent samples are mostly located in regions with low  $H_{cr}/H_c$  and  $M_r/M_s$  over 0.3. Because the Day plot was developed for rocks bearing stoichiometric magnetite, thus titanomagnetite-bearing rocks or rocks containing more oxidized phases such as hematite and maghemite may not follow the same trends (Roberts et al., 2018). Therefore, we do not show the boundaries defining SD, PSD, or MD regions in Figure 4a.

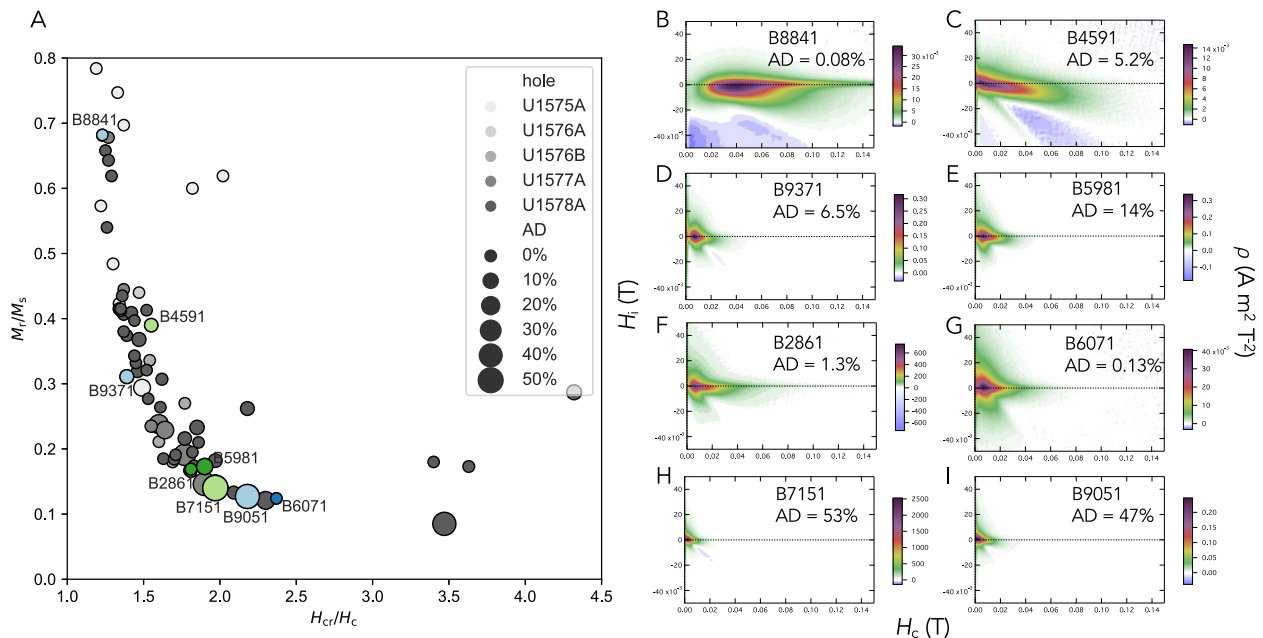
**Table 1**  
*Information About Representative Samples Presented in the Main Article and Their Amplitude-Dependence As Well As Other Rock Magnetism Characterizations*

Sample #	IODP sample identifier	Hole	Depth (mbsf)	Lithology	Deposit type	AD %	Sample #	LT $\chi-T$	HT $\chi-T$ Argon	HT $\chi-T$ air	FORC	NRM AF	NRM thermal
B8841	391-U1575A-30R-1-W 63-64	U1575A	250.13	Sparsely plagioclase-pyroxene phyrlic basalt	Sheet lava flow	0.08	B8841	X	X	X	X		
B9371	391-U1575A-39R-5-W 49-50	U1575A	308.99	Moderately to sparsely plagioclase-pyroxene phyrlic basalt, with rare olivine	Massive lava flow	6.5	B9371	X	X	X	X		
B9051	391-U1575A-37R-3-W 17-18	U1575A	296.45	Moderately plagioclase-pyroxene phyrlic basalt, with rare olivine	Sheet lava flow	46.7	B9051			X	X		
B8851	391-U1575A-29R-1-W 112-113	U1575A	245.82	Sparsely to moderately plagioclase-pyroxene-olivine phyrlic basalt	Pillow lava flows	0.36	B8851	X	X				
B6071	391-U1576B-13R-3-W 24-26	U1576B	424.33	Sparsely to moderately plagioclase-pyroxene phyrlic basalt	Massive lava flow	0.13	B6071	X	X	X	X		
B6801	391-U1576B-16R-4-W 90-92	U1576B	444.85	Plagioclase-pyroxene phyrlic basalt	Pillow lava flows	0.23	B6801	X	X	X	X	X	X
B4591	391-U1577A-21R-5-W 38-40	U1577A	174.09	Highly phyrlic plagioclase-pyroxene basalt	Massive lava flow	5.2	B4591	X	X	X	X	X	X
B4551	391-U1577A-21R-3-W 5-7	U1577A	171.49	Highly phyrlic plagioclase-pyroxene basalt	Massive lava flow	0.37	B4551	X	X				
B7151	391-U1577A-23R-4-W 4-6	U1577A	181.92	Highly phyrlic plagioclase-pyroxene-olivine basalt	Massive lava flow	53.3	B7151	X	X	X	X	X	
B7801	391-U1577A-18R-3-W 119-121	U1577A	157.49	Highly phyrlic plagioclase-pyroxene-olivine basalt	Massive lava flow	34.6	B7801	X	X	X	X	X	X
B5981	391-U1578A-48R-3-W 79-81	U1578A	391.32	Highly phyrlic plagioclase-pyroxene-olivine basalt	Massive lava flow	13.9	B5981	X	X	X	X	X	X
B2861	391-U1578A-34R-2-W 26-28	U1578A	292.52	Highly phyrlic plagioclase basalt	Pillow lava flows	1.3	B2861	X	X	X	X	X	X
B2571	391-U1578A-22R-2-W 5-7	U1578A	197.39	Aphyric to sparsely phyrlic plagioclase basalt	Pillow lava flows	2.7	B2571	X	X			X	
B3141	391-U1578A-24R-2-W 15-17	U1578A	214.65	Highly phyrlic plagioclase-pyroxene basalt	Pillow lava flows	0.2	B3141						X
B15181	391-U1577A-23R-1-W 19-21	U1577A	178.59	Sparsely phyrlic plagioclase-olivine basalt	Massive lava flow	18	B15181	X					X
B4821	391-U1577A-22R-2-W 115-117	U1577A	176.18	Highly phyrlic plagioclase-pyroxene-olivine basalt	Massive lava flow	24.5	B4821						X
B4711	391-U1577A-20R-4-W 93-95	U1577A	168.21	Highly phyrlic plagioclase-pyroxene basalt	Massive lava flow	20	B4711						X

Note. mbsf, meters below seafloor



**Figure 3.** Amplitude dependence versus mass-normalized susceptibility of basalt samples in this study. Plotted on margin axes are kernel distributions representing the nonparametric density distribution of bulk susceptibility and amplitude dependence, to better illustrate the abundance of samples with different  $\chi$  and AD values. The kernel density distributions use a Gaussian smoothing function and a bandwidth of 0.25.



**Figure 4.** Day plot of submarine basalts used in this study and First Order Reversal Curve (FORC) diagrams of representative samples. In the Day plot, the dot size corresponds to the magnitude of amplitude-dependence. FORC diagrams of 8 representative samples (shown with colored symbols on the Day plot) are ordered by their dominant domain states (SD-PSD-MD).



**Table 2**  
*Hysteresis Parameters of Representative Samples*

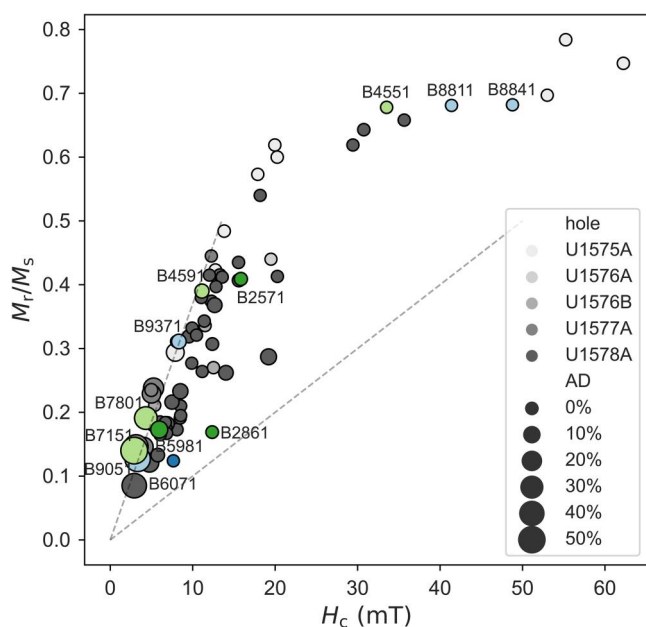
Sample #	$M_r$ (mAm <sup>2</sup> /kg)	$M_s$ (mAm <sup>2</sup> /kg)	$H_c$ (mT)	$H_{cr}$ (mT)	$H_{cr}/H_c$	$M_r/M_s$	AD %
B8841	158.5	232.3	48.78	60.19	1.23	0.682	0.08
B9371	273.8	879.6	8.32	11.57	1.39	0.311	6.5
B9051	120.5	951.9	3.318	7.239	2.18	0.127	46.7
B8851	162.6	207.4	55.24	65.64	1.19	0.784	0.36
B6071	134.4	1,083	7.654	18.15	2.37	0.124	0.13
B6801	153.8	458.3	11.5	17.7	1.54	0.336	0.23
B4591	177.7	456.2	11.12	17.23	1.55	0.390	5.2
B4551	98.07	144.6	33.52	42.64	1.27	0.678	0.37
B7151	123.6	885.4	2.901	5.702	1.97	0.140	53.3
B7801	188.7	989.6	4.315	7.619	1.77	0.191	34.6
B5981	214.7	1,238	5.937	11.3	1.90	0.173	13.9
B2861	179.9	1,067	12.36	22.43	1.81	0.169	1.3
B2571	227.6	557.1	15.84	22.44	1.42	0.409	2.7
B3141	203.7	535.9	11.05	15.17	1.37	0.38	0.2
B5181	186.4	815.7	5.001	8.217	1.64	0.229	18
B4821	215.3	905.5	5.25	8.426	1.6	0.238	24.5
B4711	155.5	1,063	4.051	7.975	1.97	0.146	20

The domain states can be more comprehensively understood with the FORC diagram. We interpreted the FORC diagrams following Roberts et al. (2014). We found that seven out of eight samples show evidence for a low-coercivity ( $H_c < 5$  mT) grain population that likely corresponds to MD titanomagnetite. In contrast, sample B8841 (Figure 4b) appears to be dominated by interacting SD grains that may have formed by rapid cooling of the basalt. B4591 (Figure 4c) displays a mixture of MD and SD behaviors. The remaining six samples (Figures 4d–4i) all show PSD + MD characteristics, with different  $H_c$  spreading ranges. The high  $H_c$  (>10 mT) components may represent titanomaghemite (oxidation) while low  $H_c$  (<10 mT) members are pure fresh titanomagnetites.

It is difficult to distinguish between amplitude-dependent and amplitude-independent samples solely by using a Day plot. Instead, plotting the squareness ratio ( $M_r/M_s$ ) versus coercivity provides better insight (Figure 5). For MD and PSD grains,  $M_r/M_s \approx H_c/(N \times M_s)$  (Wang & Van Der Voo, 2004), where  $N$  is the demagnetizing factor. While this equation was developed specifically for minerals rather than bulk rocks,  $M_r/M_s$  and  $H_c$  remain the same for a rock and the magnetic minerals within it (i.e., these parameters have no concentration-dependence). Therefore, we can use the rock  $M_r/M_s$  and  $H_c$  data to infer  $M_s$  values for the magnetic grains inside a rock. Using the above expression, we can see that the slope in the squareness versus coercivity plot is inversely correlated with  $N \times M_s$ . If we assume that the magnetic minerals in all of our basalt samples have similar  $N$  values, samples with a high slope (left side) on the squareness versus coercivity plot should be associated with low  $M_s$  values. These high-slope samples contain high-Ti titanomagnetites that display significant amplitude-dependence. In contrast, samples located toward the lower-slope end-member line should have low  $M_s$  values, which likely indicates varying degrees of oxidation and/or lower Ti contents.

### 3.2. Low- and High-Temperature Rock Magnetic Measurements

High-temperature  $\chi$ - $T$  curves measured in air were all irreversible due to oxidation-related thermal alteration. Thus, the focus here is on low-temperature results as well as  $\chi$ - $T$  curves obtained using an Ar atmosphere. No Verwey or Morin transitions were observed in the low-temperature measurements. We observed peaks around 130–200 K that may indicate hemo-ilmenite (ilmenite-hematite solid solution, with near-ilmenite composition) (Engelmann et al., 2010; Lattard et al., 2006) for four out of 35 samples (Figures 6e and 6f). This phase is also thermally stable up to 950 K as the peak remains unchanged in the second low-temperature measurement. For high-temperature heating (in Ar) and cooling measurements, the samples with reversible  $\chi$ - $T$  curves exhibit high



**Figure 5.** Squareness ratio ( $M_r/M_s$ ) versus coercivity for submarine basalts used in this study. Dot size represents the amplitude-dependence of magnetic susceptibility. The lower slope line represents the stoichiometric magnetite endmember, and the higher slope line represents fresh titanomagnetites ( $TM_{60}$ ) (Wang & Van Der Voo, 2004). Sample data plotted between these lines may indicate SD grains with varying degrees of oxidation and/or lower Ti content than  $TM_{60}$ . The upper and lower slope lines are not plotted for  $M_r/M_s > 0.5$  because the trendlines are only applicable to MD grains ( $M_r/M_s < 0.5$ ).

amplitude-dependence (Figures 6a and 6b, Group 1). The amplitude-independent samples exhibit alteration/inversions during heating and their  $\chi$ - $T$  curves are not reversible. The  $\chi$ - $T$  behaviors of samples with irreversible behavior can be classified into three groups (Figure 6). Group 2 (Figures 6e and 6h) represents samples displaying two stages of inversion. The first stage begins at  $\sim 130^\circ\text{C}$  during heating and ends with magnetite formation at  $\sim 650^\circ\text{C}$  (except for B5981, see Figure 6e), while the second one appears during the cooling stage at  $\sim 200^\circ\text{C}$ . Group 3 (Figures 6i–6l) represents samples with significant magnetite formation during heating experiments and a drastic susceptibility increase ( $>2$  times) after cooling. This group shows no humps in the cooling curves. Group 4 (Figures 6c and 6d) represents samples with observable but minor thermal alteration during heating experiments. Their magnetic susceptibility does not change drastically after heating. Among the 35  $\chi$ - $T$  curves, 13 can be classified into Group 2, 13 belong to Group 3 and 4 falls into Group 4. The remaining five samples display reversible  $\chi$ - $T$  behaviors (Group 1).

### 3.3. Demagnetization Experiments

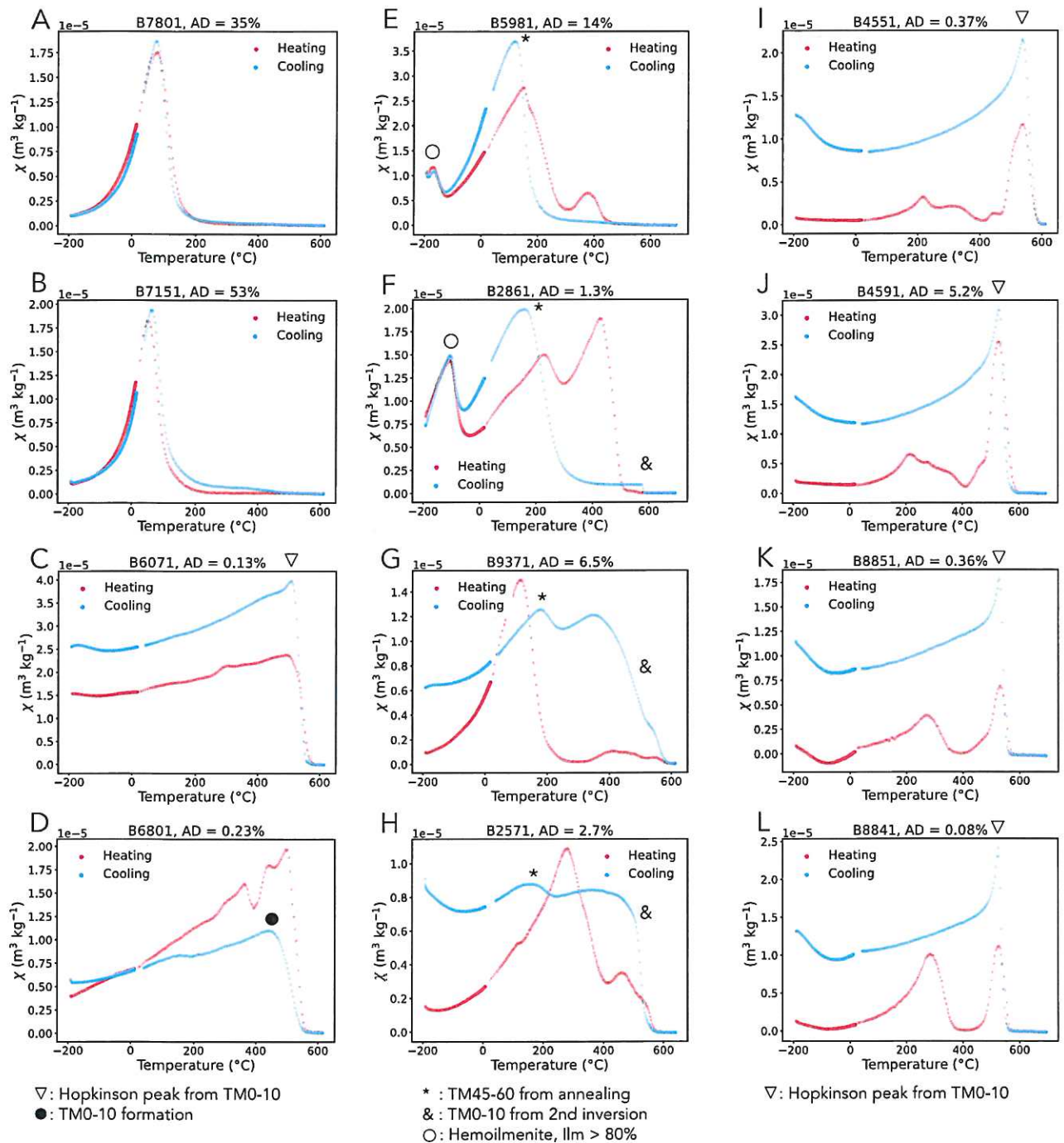
For NRM demagnetization results from our sister specimen analysis, Sample B7151 (Figure 7a) has a clear low-coercivity overprint, likely from rotary coring (Acton et al., 2002). Conversely, Sample B5981 (Figure 7b) shows a clear characteristic component in both AF and thermal treatments, without much overprint. The high-temperature component appears to be noisier due to thermal alteration at  $\sim 400^\circ\text{C}$ . This alteration is also observed at a similar temperature in the same sample's  $\chi$ - $T$  curve (Figure 6e). The AF demagnetization tests for B4591 and B2861 (Figures 7c and 7d) seem to work better than the thermal demagnetization, but this is likely due to the precision and noise level of different magnetometers used.

Additional shipboard thermal demagnetization results revealed that amplitude-dependent samples generally showed higher NRM values and more significant drilling-induced magnetic overprints than amplitude-independent samples (Figure 8). While drilling-related overprints can be removed by thermal demagnetization to  $\sim 200^\circ\text{C}$ , resolving the remaining magnetization (blocked  $< \sim 350^\circ\text{C}$  in amplitude-dependent samples B5181, B4821, and B4711, Figures 8a–8c) requires fine thermal steps. Drilling related overprint can also be seen in amplitude independent samples (sample B3141, Figure 8d) but it is not a significant part of the NRM.

## 4. Discussion

### 4.1. Bulk Susceptibility, Amplitude-Dependence, and Basalt Lithology

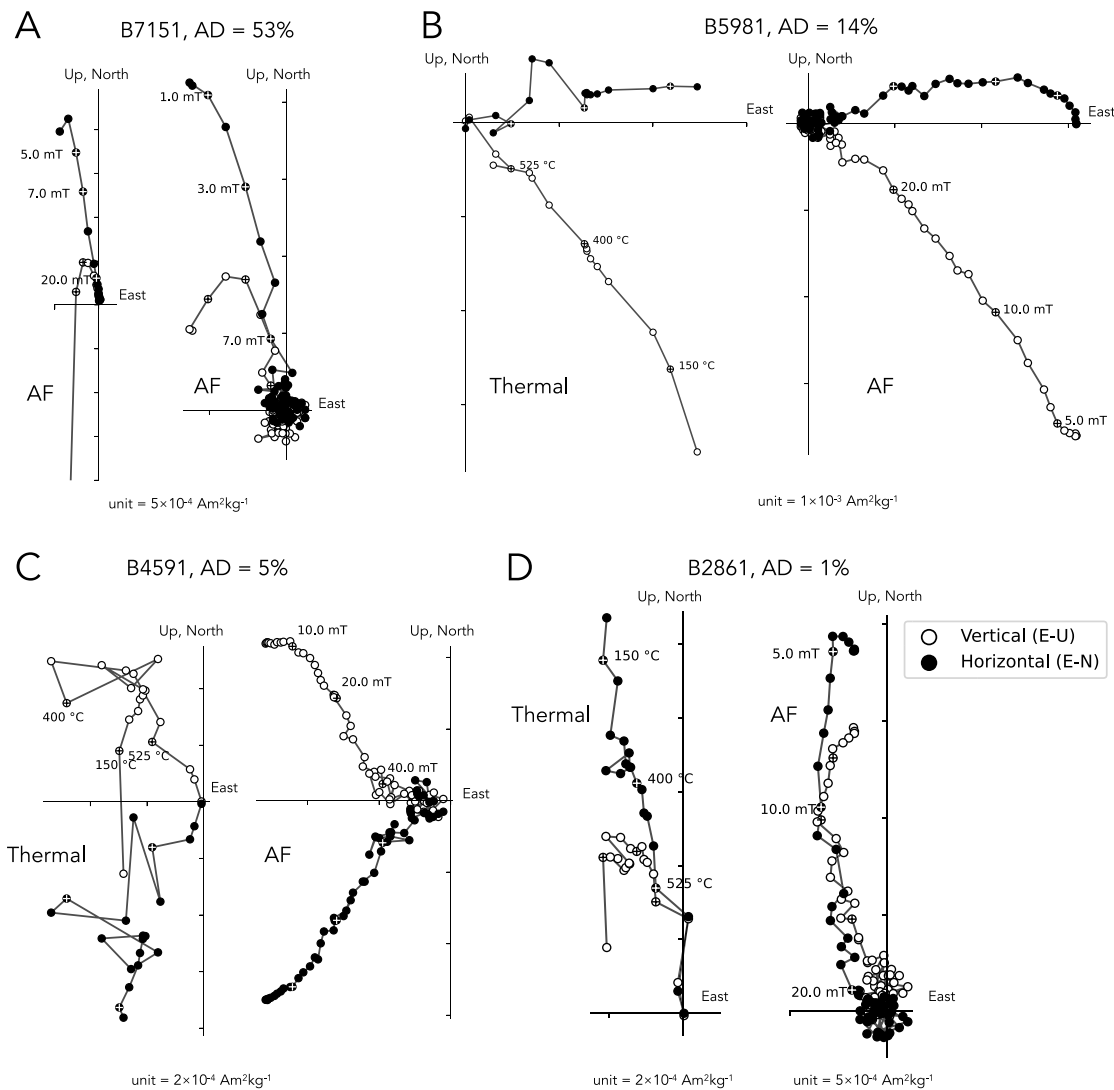
We observed that the MS amplitude-dependent samples are found only in massive basalt flows. The bulk MS values for amplitude-dependent samples are also higher than the average MS value of samples from massive flows (Figure 3). These correlations could be related to two factors. First, the amplitude-dependent samples are MD, which suggests that they might contain large grains crystallized at slow cooling rates that are most likely to occur in the interiors of massive flow units. This distance from flow boundaries will also mitigate fluid-rock interactions and preserve fresher magnetic minerals. Conversely, pillow lavas do not exhibit amplitude-dependence, probably due to rapid cooling that produced finer-grained magnetic minerals or seawater alteration. Second, the MS value can be boosted by thermal relaxation ( $\sim 1$  order of magnitude increase) when the mineral is measured at a temperature just below its Curie temperature (See Figures 6a and 6b). The thermal energy helps to overcome the magnetic anisotropy barrier and more magnetization is aligned with the applied field. Therefore, when comparing MS measured at room temperature, samples with lower  $T_C$  (especially those with  $T_C < 130^\circ\text{C}$ ), may have augmented susceptibility owing to this thermal boosting effect. The MD high-Ti titanomagnetite-bearing samples have low  $T_C$  and therefore could exhibit higher than average MS values.



**Figure 6.** High-temperature thermomagnetic  $\chi$ - $T$  curves of representative samples measured in Ar. Labels used in the figure:  $\nabla$ —indicative of SD magnetite formation from Hopkinson peak;  $\bullet$ —magnetite formation without Hopkinson peak, likely larger grain size;  $\&$ —the second stage titanomaghemite inversion product  $TM_{0-10}$ ; \*—final high-temperature annealing product  $TM_{50-65}$ ;  $\circ$ —low  $T_C$  Hemoilmenite with >80% ilmenite component.

#### 4.2. Thermomagnetic Results

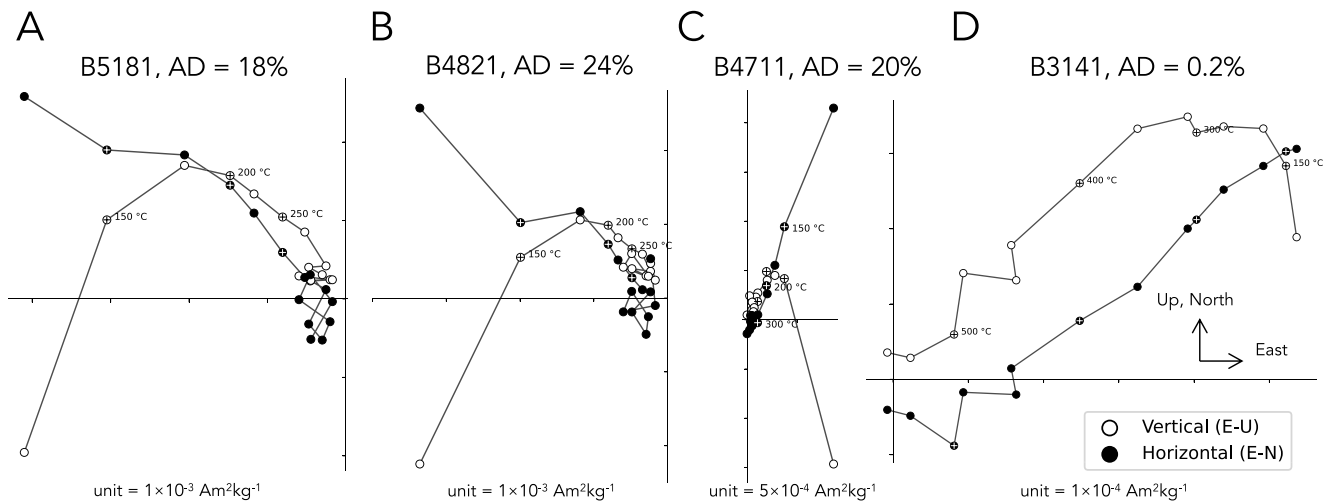
We found a clear trend that the reversible  $\chi$ - $T$  behaviors are well correlated with high amplitude dependence (AD > 30%) (Figures 6a and 6b, Group 1), while the less amplitude-dependent samples (AD < 30%) all showed irreversible  $\chi$ - $T$  curves. We can generally categorize the irreversible curves into several subgroups and provide a



**Figure 7.** Zijderveld plots of alternating field and thermal demagnetization of NRM for selected basalt samples. For each sample, the left plot is measured from an oriented cube sample during International Ocean Discovery Program Expedition 391 shipboard paleomagnetic measurements, whereas the right plot is obtained from unoriented rock chips. Note that data from the unoriented chips were rotated to align their characteristic remanent magnetization directions (obtained using principal component analysis) with those of their paired oriented samples. White and black dots represent the remaining magnetization vector projected onto the vertical and horizontal planes, respectively. Dots with a cross inside correspond to specific labeled steps.

short explanation. The reader can refer to previous  $M_s$ - $T$ ,  $\chi$ - $T$  studies (Beske-Diehl, 1990; Kontny et al., 2003; Özdemir, 1987) for thermal behaviors of altered basalts as this is not the focus of this study.

Samples B5981, (AD = 14%), B9371 (AD = 6.5%), B2571 (AD = 3%), B2861 (AD = 1%) (Figures 6e–6h, Group 2), have  $\chi$ - $T$  curves in which the cooling stage (marked with “\*”) behaves similarly to the fresh samples (Samples B7151 and B7801, Figures 6a and 6b, Group 1) (low  $T_C$  150–250°C component identifiable in cooling curve). These samples display significant offset of  $T_C$ s during heating and cooling stages, which has also been observed in pyroclastic deposits containing titanomagnetites (Dudzisz et al., 2022). This is believed to be indicative of subtle maghemitization induced nanoscale chemical clustering in titanomagnetites (Bowles et al., 2019). These four samples are likely early-stage weathering products of relatively slow-cooled basalts with high Ti content. Samples B6071 and B6801 (Figures 6c and 6d, Group 4) are representative of basalts at the final stage of maghemitization/exsolution, in which the magnetic minerals are mostly dominated by maghemite or even magnetite. Samples B4551, B4591, B8851, and B8841 (Figures 6i–6l, Group 3) belong to the group in the



**Figure 8.** Additional thermal demagnetization results from International Ocean Discovery Program Expedition 391 shipboard measurements. White and black dots represent the remaining magnetization vector projected onto the vertical and horizontal planes, respectively. Dots with a cross inside correspond to specific labeled steps.

intermediate stage of maghemitization with fine-grained (SD or SD + PSD) titanomagnetites. The  $\chi$ - $T$  curves of these samples display complete inversion to magnetite during heating (evidenced by no humps in the cooling curves), and significant increases in susceptibility after conversion. The Group 3 samples with an intermediate degree of maghemitization show higher coercivity than those of early (Group 2) or final (Group 4) stage basalts (Table 2), consistent with previous reports (Özdemir & O'Reilly, 1982).

The observed magnetic mineralogy variation in submarine basalts is difficult to infer from hand sample inspection or field observations. For example, fresh basalts with primary titanomagnetites and reversible  $\chi$ - $T$  curves, can be found in all types of subaerial (aa, pahoehoe) and submarine (massive flow, pillows and intrusive rocks) basalts (Kontny et al., 2003). The oxidized endmember (marked as high-temperature alteration in (Kontny et al., 2003)) can also be found in all kinds of lithologies. In our sample set, we commonly found that samples (e.g., B2861, B6081, and B7641) labeled as “fresh” by core describers during IODP Expedition 391 (Sager et al., 2022, 2023) show non-reversibility in  $\chi$ - $T$  experiments, which indicates alteration of magnetic minerals. Thus, information about the freshness level of titanomagnetite, which is essential for deciding upon demagnetization protocols, requires additional characterization. How amplitude-dependence of MS can be used for this purpose is discussed in the later sections.

### 4.3. Implication for Demagnetization Methods

Ideally, choosing between AF and thermal demagnetization methods for a given sample set requires information about the thermal stability, Curie temperature and mean coercivity of magnetic minerals in each specimen. Amplitude-dependence of MS can correlate well with these properties. High amplitude-dependence implies that samples have low coercivities and low Curie temperatures, suggesting that AF is likely to be a successful demagnetization method. The ability of most commercial AF-demagnetizers to set fine demagnetization increments, particularly when in-line with the magnetometer, makes this the preferred method for such samples. On the other hand, thermal demagnetization with fine temperature steps on the order of a few  $^{\circ}\text{C}$  below  $250^{\circ}\text{C}$  may also work, but setting an accurate temperature in such a low temperature range has been a technical difficulty for many paleomagnetic ovens, which tend to over-shoot the set temperature. Amplitude-independent samples are likely to have higher coercivities and higher Curie temperatures but are likely to be thermally unstable (particularly if samples are heated in air). In this case, both AF and thermal methods may be appropriate. However, for severely oxidized samples (e.g., Sample B4591 in Figure 6j), thermal demagnetization may not provide meaningful results due to alteration during high-temperature treatment in air. It appears that samples with moderate amplitude-dependence (5%–20%) are the most ideal samples for paleomagnetism. The moderate

amplitude-dependence indicates some maghemitization, but such samples are not completely oxidized. Partial maghemitization produces enhanced coercivity and  $T_C$ , so more AF or thermal steps can be performed and used for directional determination via principal component analysis.

The protocol presented here could also potentially help to exclude samples from paleointensity studies (Figures 8a–8c). The basalts with  $TM_{50-70}$  with most significant amplitude-dependence may not be ideal for paleointensity experiments because: (a) The low Curie temperatures of such basalts prevent multiple demagnetization and remagnetization steps at precisely controlled temperatures, especially in cases where paleomagnetic ovens are susceptible to overshooting the setpoint value at low temperatures below 200°C; (b) Such basalts may also exhibit self-reversal behavior at ~300–550°C due to inversion of titanomagnetite. The magnetite formed during inversion acquires a magnetization antiparallel to the applied field (Pan et al., 2006). This inversion could occur if fresh samples are heated in air or a weathered sample heated in either air or argon atmosphere.

#### 4.4. Strengths and Weaknesses of AD-Based Pre-Screening

The proposed protocol is fast (2 min per sample), and non-destructive to the magnetic remanence recorded in the samples. This technique has a clear advantage over methods like thermomagnetic curves ( $M_s-T$  or  $\chi-T$ ) or domain state determinations (hysteresis or FORC measurements), which typically require minutes to several hours for each specimen, and destroy the natural remanent magnetization of the specimen. Our method only requires room-temperature susceptibility measurements with varying amplitude-amplitude. Such measurements can be performed using the Kappabridge susceptibility meters (without the use of gas) that are common in paleomagnetism labs as well as on-board the *JOIDES Resolution* drilling vessel, unlike more sophisticated and expensive instruments such as vibrating-sample magnetometers.

Given the relatively high failure rate of demagnetization experiments performed on discrete samples in the context of IODP shipboard paleomagnetism protocols, our method aids in providing valuable information for optimizing the demagnetization protocols. Admittedly, this is a preliminary characterization and only works for the Fe-Ti-O ternary system. Other complex mineralogy cannot be resolved through this method, especially for the low-AD or amplitude-independent samples (Bowles et al., 2019; Dudzisz et al., 2022; Lied et al., 2020).

### 5. Conclusions

We found that the amplitude-dependence of MS can be used to provide a magnetically nondestructive preliminary characterization of the magnetic mineralogy of submarine basalts. This pre-screening protocol can help decide whether to use AF or thermal demagnetization methods when conducting paleomagnetic studies in situations where complex preliminary rock magnetic measurements cannot be performed. Amplitude-dependent submarine basalt samples are associated with fresh MD Ti-rich magnetite with relatively low coercivities and unblocking temperatures. Therefore, AF demagnetization is likely to be more successful than thermal demagnetization in such cases, although thermal demagnetization may also work if finely spaced thermal steps are used at low temperatures (<300°C). In contrast, amplitude-independent samples may contain either fine-grained titanomagnetite or may have been oxidized (maghemitized) by fluid-rock interactions with seawater. Because of the moderate coercivities and high unblocking temperatures of these rocks, amplitude-independent samples may be treated by either thermal or AF demagnetization methods.

#### Data Availability Statement

Data used in this study are openly available in the Zenodo repository (Yang et al., 2023).

### References

- Acton, G. D., Okada, M., Clement, B. M., Lund, S. P., & Williams, T. (2002). Paleomagnetic overprints in ocean sediment cores and their relationship to shear deformation caused by piston coring. *Journal of Geophysical Research*, 107(4), EPM 3-1–EPM 3-15. <https://doi.org/10.1029/2001JB000518>
- Banerjee, S. K. (1971). New grain size limits for palaeomagnetic stability in haematite. *Nature Physical Science*, 232(27), 15–16. <https://doi.org/10.1038/physci232015a0>
- Beske-Diehl, S. J. (1990). Magnetization during low-temperature oxidation of seafloor basalts: No large scale chemical remagnetization. *Journal of Geophysical Research*, 95(B13), 21413–21432. <https://doi.org/10.1029/JB095iB13p21413>
- Bilardello, D. (2023). A review of the low temperature AC susceptibility frequency-dependence of multidomain (titano)magnetite. *The IRM Quarterly*, 32(4).

#### Acknowledgments

We thank two reviewers Marco Maffione and Agnes Kontny for their constructive comments that greatly improved our manuscript. This research used samples and data provided by the IODP. Part of the present work was performed by H. Yang as a US Visiting Student Fellow at the IRM at the University of Minnesota. The IRM is a US National Multi-user Facility supported through the Instrumentation and Facilities program of the National Science Foundation, Earth Sciences Division, award NSF-EAR 2153786, and by funding from the University of Minnesota. This is IRM publication #2301. This research was also supported by U.S. Science Support Program Post-Expedition Awards to S. Tikoo, W. Sager, K. Gastra, and S. Thoram and U.S. National Science Foundation Grants to S. Tikoo (award number 2232971) and W. Sager (award number 2232970). We thank the IODP for supporting Expedition 391, as well as the crew of the *D/V JOIDES Resolution* and the IODP technical staff for their role in obtaining samples and assisting with preliminary analyses on board. The Contribution of DMB, EP, MW was supported by UK IODP NERC grants. S. Homrighausen was funded by the Deutsche Forschungsgemeinschaft (DFG) Grant 439265336.

- Bilardello, D., & Roberts, A. P. (2020). Practical magnetism IV: Feats and challenges in quantifying hematite with magnetic methods. *The IRM Quarterly*, 30(3).
- Bleil, U., & Petersen, N. (1983). Variations in magnetization intensity and low-temperature titanomagnetite oxidation of ocean floor basalts. *Nature*, 301(5899), 384–388. <https://doi.org/10.1038/301384a0>
- Bono, R. K., Tarduno, J. A., & Bunge, H.-P. (2019). Hotspot motion caused the Hawaiian-Emperor Bend and LLSVPs are not fixed. *Nature Communications*, 10(1), 3370. <https://doi.org/10.1038/s41467-019-11314-6>
- Bono, R. K., Tarduno, J. A., Nimmo, F., & Cottrell, R. D. (2019). Young inner core inferred from Ediacaran ultra-low geomagnetic field intensity. *Nature Geoscience*, 12(2), 143–147. <https://doi.org/10.1038/s41561-018-0288-0>
- Bowles, J. A., & Jackson, M. J. (2016). Effects of titanomagnetite reordering processes on thermal demagnetization and paleointensity experiments. *Geochemistry, Geophysics, Geosystems*, 17(12), 4848–4858. <https://doi.org/10.1002/2016GC006607>
- Bowles, J. A., Lappe, S.-C. L. L., Jackson, M. J., Arenholz, E., & van der Laan, G. (2019). Curie temperature enhancement and cation ordering in titanomagnetites: Evidence from magnetic properties, XMCD, and Mössbauer spectroscopy. *Geochemistry, Geophysics, Geosystems*, 20(5), 2272–2289. <https://doi.org/10.1029/2019GC008217>
- Butler, R. F., & Banerjee, S. K. (1975). Theoretical single-domain grain size range in magnetite and titanomagnetite. *Journal of Geophysical Research*, 80(29), 4049–4058. <https://doi.org/10.1029/JB080i029p04049>
- Clark, D. A. (2016). Field-dependent susceptibility of rocks and ores - Implications for magnetic petrophysics and magnetic modelling. *ASEG Extended Abstracts*, 2016, 1–9. <https://doi.org/10.1071/ASEG2016ab233>
- Coe, R. S. (1967). The determination of paleo-intensities of the Earth's magnetic field with emphasis on mechanisms which could cause non-ideal behavior in Thellier's method. *Journal of Geomagnetism and Geoelectricity*, 19(3), 157–179. <https://doi.org/10.5636/jgg.19.157>
- De Wall, H. (2000). The field-dependence of AC susceptibility in titanomagnetites: Implications for the anisotropy of magnetic susceptibility. *Geophysical Research Letters*, 27(16), 2409–2411. <https://doi.org/10.1029/2000GL008515>
- Dudzisz, K., Kontny, A., & Alva-Valdivia, L. M. (2022). Curie temperatures and emplacement conditions of pyroclastic deposits from Popocatepetl volcano, Mexico. *Geochemistry, Geophysics, Geosystems*, 23(8), e2022GC010340. <https://doi.org/10.1029/2022GC010340>
- Dunlop, D. J. (1973). Superparamagnetic and single-domain threshold sizes in magnetite. *Journal of Geophysical Research*, 78(11), 1780–1793. <https://doi.org/10.1029/JB078i011p01780>
- Dunlop, D. J., & Özdemir, Ö. (1997). *Rock magnetism: Fundamentals and frontiers*. Cambridge University Press.
- Engelmann, R., Kontny, A., Lattard, D., & Sauerzapf, U. (2010). Low-temperature magnetometry of synthetic Fe-Ti oxide assemblages. *Journal of Geophysical Research*, 111(B12), B12S28. <https://doi.org/10.1029/2006JB004591>
- Furuta, T. (1993). Magnetic properties and ferromagnetic mineralogy of oceanic basalts. *Geophysical Journal International*, 113(1), 95–114. <https://doi.org/10.1111/j.1365-246X.1993.tb02531.x>
- Gee, J. S., & Kent, D. V. (2007). Source of oceanic magnetic anomalies and the geomagnetic polarity timescale. <https://doi.org/10.1016/B978-044452748-6.00097-3>
- Gunnlaugsson, H. P., Helgason, Ö., Kristjánsson, L., Nørnberg, P., Rasmussen, H., Steinþórsson, S., & Weyer, G. (2006). Magnetic properties of olivine basalt: Application to Mars. *Physics of the Earth and Planetary Interiors*, 154(3–4), 276–289. <https://doi.org/10.1016/j.pepi.2005.09.012>
- Hamilton, M. (2021). Investigation of strongly negative field dependence of susceptibility in the subsurface of northeastern Oklahoma. *The IRM Quarterly*, 31, 2–5.
- Harrison, R. J., & Feinberg, J. M. (2008). FORCinel: An improved algorithm for calculating first-order reversal curve distributions using locally weighted regression smoothing. *Geochemistry, Geophysics, Geosystems*, 9(5), Q05016. <https://doi.org/10.1029/2008GC001987>
- Jackson, M., Moskowitz, B., Rosenbaum, J., & Kissel, C. (1998). Field-dependence of AC susceptibility in titanomagnetites. *Earth and Planetary Science Letters*, 157(3–4), 129–139. [https://doi.org/10.1016/S0012-821X\(98\)00032-6](https://doi.org/10.1016/S0012-821X(98)00032-6)
- Kirschvink, J., Kopp, R. E., Raub, T. D., Baumgartner, C. T., & Holt, J. W. (2008). Rapid, precise, and high-sensitivity acquisition of paleomagnetic and rock-magnetic data: Development of a low-noise automatic sample changing system for superconducting rock magnetometers. *Geochemistry, Geophysics, Geosystems*, 9(5), Q05Y01. <https://doi.org/10.1029/2007GC001856>
- Kirschvink, J. L. (1980). The least-squares line and plane and the analysis of palaeomagnetic data. *Geophysical Journal International*, 62(3), 699–718. <https://doi.org/10.1111/j.1365-246X.1980.tb02601.x>
- Kontny, A., Vahle, C., & de Wall, H. (2003). Characteristic magnetic behavior of subaerial and submarine lava units from the Hawaiian Scientific Drilling Project (HSDP-2). *Geochemistry, Geophysics, Geosystems*, 4(2), 8703. <https://doi.org/10.1029/2002GC000304>
- Kreemer, C., & Gordon, R. G. (2014). Pacific plate deformation from horizontal thermal contraction. *Geology*, 42(10), 847–850. <https://doi.org/10.1130/G35874.1>
- Lattard, D., Engelmann, R., Kontny, A., & Sauerzapf, U. (2006). Curie temperatures of synthetic titanomagnetites in the Fe-Ti-O system: Effects of composition, crystal chemistry, and thermomagnetic methods. *Journal of Geophysical Research*, 111(B12), B12S28. <https://doi.org/10.1029/2006JB004591>
- Lied, P., Kontny, A., Nowaczyk, N., Mrlina, J., & Kämpf, H. (2020). Cooling rates of pyroclastic deposits inferred from mineral magnetic investigations: A case study from the Pleistocene Mytina Maar (Czech Republic). *International Journal of Earth Sciences*, 109(5), 1707–1725. <https://doi.org/10.1007/s00531-020-01865-1>
- Moskowitz, B. M. (1980). Theoretical grain size limits for single-domain, pseudo-single-domain and multi-domain behavior in titanomagnetite ( $x = 0.6$ ) as a function of low-temperature oxidation. *Earth and Planetary Science Letters*, 47(2), 285–293. [https://doi.org/10.1016/0012-821X\(80\)90045-X](https://doi.org/10.1016/0012-821X(80)90045-X)
- Moskowitz, B. M., Jackson, M., & Chandler, V. (2015). Geophysical properties of the near-surface Earth: Magnetic properties. In *Treatise on Geophysics* (pp. 139–174). Elsevier. <https://doi.org/10.1016/B978-0-444-53802-4.00191-3>
- Özdemir, Ö. (1987). Inversion of titanomagnethites. *Physics of the Earth and Planetary Interiors*, 46(1–3), 184–196. [https://doi.org/10.1016/0031-9201\(87\)90181-6](https://doi.org/10.1016/0031-9201(87)90181-6)
- Özdemir, Ö., & O'Reilly, W. (1982). Magnetic hysteresis properties of synthetic monodomain titanomagnethites. *Earth and Planetary Science Letters*, 57(2), 437–447. [https://doi.org/10.1016/0012-821X\(82\)90162-5](https://doi.org/10.1016/0012-821X(82)90162-5)
- Pan, Y., Liu, Q., Deng, C., Qin, H., & Zhu, R. (2006). Thermally induced inversion of Al-substituted titanomagnetite in basalts: Evidence for partial self-reversal. *Journal of Geophysical Research*, 111(B12), B12S29. <https://doi.org/10.1029/2006JB004576>
- Roberts, A. P., Heslop, D., Zhao, X., & Pike, C. R. (2014). Understanding fine magnetic particle systems through use of first-order reversal curve diagrams: FORC diagrams. *Reviews of Geophysics*, 52(4), 557–602. <https://doi.org/10.1002/2014RG000462>
- Roberts, A. P., Pike, C. R., & Verosub, K. L. (2000). First-order reversal curve diagrams: A new tool for characterizing the magnetic properties of natural samples. *Journal of Geophysical Research*, 105(B12), 28461–28475. <https://doi.org/10.1029/2000JB900326>

- Roberts, A. P., Tauxe, L., Heslop, D., Zhao, X., & Jiang, Z. (2018). A critical appraisal of the “Day” diagram. *Journal of Geophysical Research: Solid Earth*, 123(4), 2618–2644. <https://doi.org/10.1002/2017JB015247>
- Roberts, A. P., Zhao, X., Heslop, D., Abrajevitch, A., Chen, Y.-H., Hu, P., et al. (2020). Hematite ( $\alpha\text{-Fe}_2\text{O}_3$ ) quantification in sedimentary magnetism: Limitations of existing proxies and ways forward. *Geoscience Letters*, 7(1), 8. <https://doi.org/10.1186/s40562-020-00157-5>
- Sager, W., Hoernle, K., & Höfig, T. W. (2022). International Ocean Discovery Program Expedition 391 Preliminary Report: Walvis Ridge Hotspot. *International Ocean Discovery Program*. <https://doi.org/10.14379/iodp.pr.391.2022>
- Sager, W., Hoernle, K., & Höfig, T. W. (2023). *Proceedings of the International Ocean Discovery Program* (Vol. 391). Walvis Ridge Hotspot. <https://doi.org/10.14379/iodp.proc.391.2023>
- Sager, W. W. (2007). Divergence between paleomagnetic and hotspot-model-predicted polar wander for the Pacific plate with implications for hotspot fixity. In *Special Paper 430: Plates, Plumes and Planetary Processes* (pp. 335–357). Geological Society of America. [https://doi.org/10.1130/2007.2430\(17\)](https://doi.org/10.1130/2007.2430(17))
- Sager, W. W., & Koppers, A. A. P. (2000). Late Cretaceous polar wander of the Pacific plate: Evidence of a rapid true polar wander event. *Science*, 287(5452), 455–459. <https://doi.org/10.1126/science.287.5452.455>
- Soffel, H. (1977). Pseudo-single-domain effects and single-domain multidomain transition in natural pyrrhotite deduced from domain structure observations. *Journal of Geophysics*, 42(1), 351–359.
- Tarduno, J. A., Duncan, R. A., Scholl, D. W., Cottrell, R. D., Steinberger, B., Thordarson, T., et al. (2003). The Emperor Seamounts: Southward motion of the Hawaiian hotspot plume in Earth’s mantle. *Science*, 301(5636), 1064–1069. <https://doi.org/10.1126/science.1086442>
- Tauxe, L. (2006). Long-term trends in paleointensity: The contribution of DSDP/ODP submarine basaltic glass collections. *Physics of the Earth and Planetary Interiors, ODP Contributions to Paleomagnetism*, 156(3–4), 223–241. <https://doi.org/10.1016/j.pepi.2005.03.022>
- Tauxe, L., & Staudigel, H. (2004). Strength of the geomagnetic field in the Cretaceous Normal Superchron: New data from submarine basaltic glass of the Troodos Ophiolite. *Geochemistry, Geophysics, Geosystems*, 5(2), Q02H06. <https://doi.org/10.1029/2003GC000635>
- Thellier, E. (1959). Sur l’intensité du champ magnétique terrestre dans le passé historique et géologique. *Annales Geophysicae*, 15, 285–376.
- Ustra, A., Mendonça, C. A., Leite, A., Jovane, L., & Trindade, R. I. F. (2018). Quantitative interpretation of the magnetic susceptibility frequency dependence. *Geophysical Journal International*, 213(2), 805–814. <https://doi.org/10.1093/gji/ggy007>
- Vahle, C., & Kontny, A. (2005). The use of field dependence of AC susceptibility for the interpretation of magnetic mineralogy and magnetic fabrics in the HSDP-2 basalts, Hawaii. *Earth and Planetary Science Letters*, 238(1–2), 110–129. <https://doi.org/10.1016/j.epsl.2005.07.010>
- Vine, F. J., & Matthews, D. H. (1963). Magnetic anomalies over oceanic ridges. *Nature*, 199(4897), 947–949. <https://doi.org/10.1038/199947a0>
- Wang, D., & Van Der Voo, R. (2004). The hysteresis properties of multidomain magnetite and titanomagnetite/titanomaghemite in mid-ocean ridge basalts. *Earth and Planetary Science Letters*, 220(1–2), 175–184. [https://doi.org/10.1016/S0012-821X\(04\)00052-4](https://doi.org/10.1016/S0012-821X(04)00052-4)
- Worm, H.-U., Clark, D., & Dekkers, M. J. (1993). Magnetic susceptibility of pyrrhotite: Grain size, field and frequency dependence. *Geophysical Journal International*, 114(1), 127–137. <https://doi.org/10.1111/j.1365-246X.1993.tb01472.x>
- Xu, W., Peacor, D. R., Dollase, W. A., Voo, R. V. D., & Beaubouef, R. (1997). Transformation of titanomagnetite to titanomaghemite: A slow, two-step, oxidation-ordering process in MORB. *American Mineralogist*, 82(11–12), 1101–1110. <https://doi.org/10.2138/am-1997-11-1207>
- Yang, H., Tikoo, S. M., Carvallo, C., Bilardello, D., Soliheld, P., Gaastra, K. M., et al. (2023). Preliminary characterization of submarine basalt magnetic mineralogy using amplitude-dependence of magnetic susceptibility [Dataset]. Zenodo. <https://doi.org/10.5281/zenodo.8310754>
- Zhou, W., Van der Voo, R., Peacor, D. R., Wang, D., & Zhang, Y. (2001). Low-temperature oxidation in MORB of titanomagnetite to titanomaghemite: A gradual process with implications for marine magnetic anomaly amplitudes. *Journal of Geophysical Research*, 106(B4), 6409–6421. <https://doi.org/10.1029/2000JB900447>
- Zhou, W., Van der Voo, R., Peacor, D. R., & Zhang, Y. (2000). Variable Ti-content and grain size of titanomagnetite as a function of cooling rate in very young MORB. *Earth and Planetary Science Letters*, 179(1), 9–20. [https://doi.org/10.1016/S0012-821X\(00\)00100-X](https://doi.org/10.1016/S0012-821X(00)00100-X)

## Erratum

The originally published article contained a typographical error in the math in the second sentence of Section 4.4. ( $M_s\text{-}T$  or  $\square\text{-}T$ ) should be ( $M_s\text{-}T$  or  $\chi\text{-}T$ ). The error has been corrected, and this may be considered the authoritative version of record.